Charles University in Prague

Faculty of Mathematics and Physics

BACHELOR THESIS

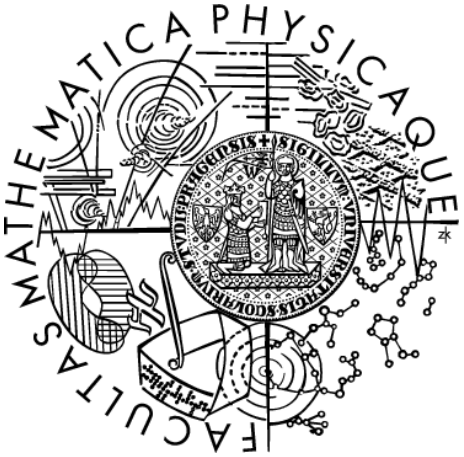

Michal Zamkovský

Spolupráce na experimentu NA62 v CERN

Collaboration on NA62 Experiment at CERN

Institute of Nuclear and Particle Physics

Supervisor of the bachelor thesis: RNDr. Karol Kampf, Ph.D.

Study programme: Physics

Specialization: Nuclear and subnuclear physics

Prague 2012

I am grateful to my supervisor in Prague Karol Kampf, to my consultant in Prague Rupert Leitner and also to my supervisor in CERN Augusto Ceccucci. Their support was priceless. The completion of this thesis would be impossible without their guidance. I also want to thank my colleagues in CERN for a lot of useful advice.

I declare that I carried out this bachelor thesis independently, and only with the cited sources, literature and other professional sources.

I understand that my work relates to the rights and obligations under the Act No. 121/2000 Coll., the Copyright Act, as amended, in particular the fact that the Charles University in Prague has the right to conclude a license agreement on the use of this work as a school work pursuant to Section 60 paragraph 1 of the Copyright Act.

In Prague date 21.5.2012 signature of the author

Název práce: Spolupráce na experimentu NA62 v CERNu

Autor: Michal Zamkovský

Ústav: Ústav jaderné a částicové fyziky

Vedoucí bakalářské práce: RNDr. Karol Kampf, Ph.D., Ústav jaderné a částicové fyziky

Abstrakt: Hlavním cílem této práce je první seznámení s experimentem NA62, který se připravuje k provozu v Evropské organizaci pro jaderný výzkum, CERN. Příprava a konstrukce nového experimentu umožňuje jedinečné zapojení se do experimentální skupiny, plné pochopení všech součástí a přípravu na příští fyzikální program. Vlastní práce má dvě části: první popisuje hlavní fyzikální motivaci a možné směry. Ve druhé části jsou shrnuté všechny důležité experimentální součásti.

Klíčová slova: kaon, CKM matice, standartní model

Title: Collaboration on NA62 Experiment at CERN

Author: Michal Zamkovský

Department: Institute of Nuclear and Particle Physics

Supervisor: RNDr. Karol Kampf, Ph.D., Institute of Nuclear and Particle Physics, MFF UK

Abstract: The primary objective of this work is first encounter with the experiment NA62 which is in the process of preparation at European organization for nuclear research, CERN. Preparations and construction of a new experiment is a unique opportunity how to become part of the experimental group, comprehensive understanding of all part and good start for the future physical program. The work has two main parts. The first part involves physical motivation and possible direction of physical program. The second part covers all important experimental sections.

Keywords: kaon, CKM matrix, Standard Model

Contents

1. Introduction

CERN, the European Organization for Nuclear Research, is one of the biggest scientific organizations specialized in fundamental physics. CERN is situated on the border between Switzerland and France, near the town Geneva. The research on individual experiments uses primary particle beams from two colliders, LHC (Large Hadron Collider) and SPS (Super Proton Synchrotron). The LHC is bigger and also uses the primary proton beam from SPS. This thesis is about the NA62 experiment, a brief introduction to its theory and description of the experimental layout, which is a follower of the previos NA48 (overview of publications [1]) and NA48/2 [2] experiments. The NA62 experiment is situated in North Area district, which is in Prévessin, France. It uses the proton beam from SPS, which is hitting the rigid berylium target, where the kaons are created. With them NA62 can fulfill its main aim, a study of rare kaon decays. In the Figure 1.1 of this page we can see the logo of the experiment, which was chosen with respect to penguin loops in quantum field theory that describes the studied processes. In the shadow of NA62 we can see also its predecessor NA48. The technical run of the experiment is planned in October 2012 and physical run, and data collection, will take place after the SPS shutdown in spring 2014.

Figure 1.1: The logo of NA62 experiment.[3]

2. Physical Motivation

2.1 Introduction

The main aim of the NA62 experiment is to measure the coefficient of V_{td} in CKM matrix with accuracy better than 10%, which will be the stringent test of Standard Model (SM). This would be accomplished by measuring the rare kaon decay $K^+ \to \pi\nu\bar{\nu}$. This decay is very interesting in sense that it contains pure $\bar{s}$ decay provided by $t, \quad \bar{t}$ pair (see Figure 2.1). This rare decay can not be measured

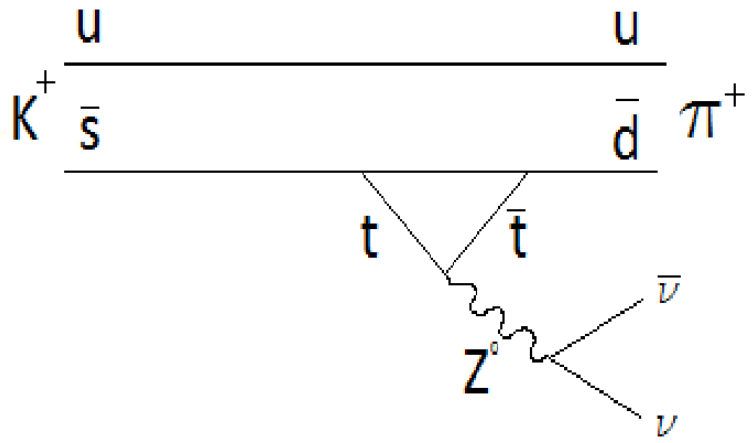

Figure 2.1: Feynman diagram of K^+ decay

directly, because we can not detect neutrinos, so we need to constrain all pions originating from other decays. However, this is very difficult, because branching ratio of $K^+ \to \pi^+\nu\bar{\nu}$ decay is $\approx 10^{-10}$ [4]. To provide successful measurement the set of detectors, described in next chapters, and appropriate configuration of triggers are needed. Triggers are based on kinematics and energy cuts. If the predictions of SM will not be in agreement, it can also point to some new physics beyond the SM. Recent experimental results from B-factories on LHCb show that flavour structure is in agreement with SM predictions. Also Supersymmetry (SUSY) has not been observed directly at LHC. Another supply to SM is assumption of Higgs observed at LHC with mass around $M_H = 125GeV/c^2$. Besides these results there is still the theoretical assumption that new physics has a supersymmetric structure. The minimum flavour-violating (MFV) SUSY is unlikely and high tan β SUSY scenarios are ruled out. So the most probable scenario

is "Natural SUSY" (see [5]), in which are supersymmetric partners $\tilde{u}$, $\tilde{d}$, $\tilde{c}$ heavy, $\tilde{b}$ not light and $\tilde{t}$ light (no significant constraint from direct SUSY searches at LHC up to now). We have to look for effects of new physics in processes sensitive to $\tilde{t}$, which can contribute to SM level only via loops. Complementary to direct search (providing by comparing coupling vs masses), Z-loop is the best place to investigate. Physics processes, where the $\tilde{t}$ can be produced are Flavour Changing Neutral Currents (FCNC) decays $B_S \to \mu\mu$ and $K \to \pi\nu\nu$, or direct production of $\tilde{t}\tilde{t}^\dagger$ via gluino (but production via gluino has too small branchig ratio and too high irreducible background from concurrent tt production). Direct production also requires high energies, which could be achieved at LHC 14 TeV [6]. The sfermion mass matrices are not necessarily diagonal (and real) in the same basis as the fermion mass matrices. Especially the trilinear A-terms (left-right mixing) can induce dangerously large flavour mixing (and complex phases) since they do not necessarily respect the hierarchy of the SM fermions (CKM matrix and up-squarks mass matrices) [7]. These conditions point towards a scenario where $K \to \pi\nu\nu$ is one of the few places where new physics can give measurable effects (if new physics is SUSY). More about the new physics models is beyond the scope of this thesis, so i will only describe the CKM matrix and outline the useful tool, called unitarity triangle.

2.2 CKM Matrix

Lagrangian for the electroweak interaction is [8]

$$\mathcal{L} = \mathcal{L}_{kin} + g(W_\mu^+ J_W^{\mu+} + W_\mu^- J_W^{\mu-} + Z_\mu^0 J_Z^\mu) + eA_\mu J_{EM}^\mu, \tag{2.1}$$

where g is constant related to the Fermi constant through $\frac{G_F}{\sqrt{2}} = \frac{g^2}{8m_W^2}$. The unitary transformation 3x3 matrices $\mathcal{U}_L, \mathcal{U}_R, \mathcal{V}_L, \mathcal{V}_R$ defined by relations [9]

$$\begin{pmatrix} d_L \\ s_L \\ b_L \end{pmatrix} = \mathcal{U}_L \begin{pmatrix} d_{0L} \\ s_{0L} \\ b_{0L} \end{pmatrix}, \qquad \begin{pmatrix} d_R \\ s_R \\ b_R \end{pmatrix} = \mathcal{U}_R \begin{pmatrix} d_{0R} \\ s_{0R} \\ b_{0R} \end{pmatrix}$$
$$\begin{pmatrix} u_L \\ c_L \\ t_L \end{pmatrix} = \mathcal{V}_L \begin{pmatrix} u_{0L} \\ c_{0L} \\ t_{0L} \end{pmatrix}, \qquad \begin{pmatrix} u_R \\ c_R \\ t_R \end{pmatrix} = \mathcal{V}_R \begin{pmatrix} u_{0R} \\ c_{0R} \\ t_{0R} \end{pmatrix} \tag{2.2}$$

cancel out of the kinetic terms, the electromagnetic current and the Z^0 boson current. For example [10]:

$$(\bar{u}_L, \bar{c}_L, \bar{t}_L)\,\gamma^\mu \begin{pmatrix} u_L \\ c_L \\ t_L \end{pmatrix} \to (\bar{u}_L, \bar{c}_L, \bar{t}_L)\,\mathcal{V}_L^\dagger \gamma^\mu \mathcal{V}_L \begin{pmatrix} u_L \\ c_L \\ t_L \end{pmatrix} = (\bar{u}_L, \bar{c}_L, \bar{t}_L)\,\gamma^\mu \begin{pmatrix} u_L \\ c_L \\ t_L \end{pmatrix}. \tag{2.3}$$

However, in the current that couplesto the W boson field, we find that the charged-current interaction written in terms of the original unphysical quark fields has the form:

$$\mathcal{L}_{CC}^{quark} = \frac{g}{\sqrt{2}}\,(\bar{u}_{0L}, \bar{c}_{0L}, \bar{t}_{0L})\,\gamma^\mu \begin{pmatrix} d_{0L} \\ s_{0L} \\ b_{0L} \end{pmatrix} W_\mu^+ + h.c. \tag{2.4}$$

and after the unitary transformation to the physical basis by $\mathcal{U}_L$ and $\mathcal{V}_L$ we obtain:

$$\mathcal{L}_{CC}^{quark} = \frac{g}{\sqrt{2}}\,(\bar{u}_L, \bar{c}_L, \bar{t}_L)\,\mathcal{V}_L^\dagger \gamma^\mu \mathcal{U}_L \begin{pmatrix} d_L \\ s_L \\ b_L \end{pmatrix} W_\mu^+ + h.c. \tag{2.5}$$

The unitary matrix $\mathbf{V} = \mathcal{V}_L^\dagger \mathcal{U}_L \neq \mathbb{1}$ is called the Cabibbo - Kobayashi - Maskawa (CKM) mixing matrix. It is 3x3 matrix with nine complex elements, so with respect to unitarity it can be parametrized by nine real numbers. However, some phase factors become physically irrelevant, as they can be absorbed into appropriate redefinitions of the quark fields. When we take only the essential part of the charged-current interaction lagrangian

$$(\bar{u}, \bar{c}, \bar{t}) \begin{pmatrix} V_{11} & V_{12} & V_{13} \\ V_{21} & V_{22} & V_{23} \\ V_{31} & V_{32} & V_{33} \end{pmatrix} \begin{pmatrix} d \\ s \\ b \end{pmatrix} \tag{2.6}$$

and factor out possible complex phase factors from CKM matrix

$$\mathbf{V} = \begin{pmatrix} e^{i\delta_{11}} & 0 & 0 \\ 0 & e^{i\delta_{21}} & 0 \\ 0 & 0 & e^{i\delta_{31}} \end{pmatrix} \begin{pmatrix} e^{-i\delta_{11}} & 0 & 0 \\ 0 & e^{-i\delta_{21}} & 0 \\ 0 & 0 & e^{-i\delta_{31}} \end{pmatrix} \begin{pmatrix} R_{11}e^{i\delta_{11}} & V_{12} & V_{13} \\ R_{21}e^{i\delta_{21}} & V_{22} & V_{23} \\ R_{31}e^{i\delta_{31}} & V_{32} & V_{33} \end{pmatrix} \tag{2.7}$$

with $R_{11}, R_{21}, R_{31}, \delta_{11}, \delta_{21}$ and δ_{31} real, we can rewrite (2.6) as

$$\left(\bar{u}e^{i\delta_{11}}, \bar{c}e^{i\delta_{21}}, \bar{t}e^{i\delta_{31}}\right) \begin{pmatrix} R_{11} & V_{12}e^{-i\delta_{11}} & V_{13}e^{-i\delta_{11}} \\ R_{21} & V_{22}e^{-i\delta_{21}} & V_{23}e^{-i\delta_{21}} \\ R_{31} & V_{32}e^{-i\delta_{31}} & V_{33}e^{-i\delta_{31}} \end{pmatrix} \begin{pmatrix} d \\ s \\ b \end{pmatrix}. \tag{2.8}$$

Similarly we obtain from

$$\begin{pmatrix} R_{11} & R_{12}e^{-i\delta_{12}} & R_{13}e^{-i\delta_{13}} \\ R_{21} & V_{22}e^{-i\delta_{21}} & V_{23}e^{-i\delta_{21}} \\ R_{31} & V_{32}e^{-i\delta_{31}} & V_{33}e^{-i\delta_{31}} \end{pmatrix} \begin{pmatrix} 1 & 0 & 0 \\ 0 & e^{-i\delta_{12}} & 0 \\ 0 & 0 & e^{-i\delta_{13}} \end{pmatrix} \begin{pmatrix} 1 & 0 & 0 \\ 0 & e^{i\delta_{12}} & 0 \\ 0 & 0 & e^{i\delta_{13},} \end{pmatrix} \quad (2.9)$$

the expression

$$\left(\bar{u}e^{i\delta_{11}}, \bar{c}e^{i\delta_{21}}, \bar{t}e^{i\delta_{31}}\right) \begin{pmatrix} R_{11} & R_{12} & R_{13} \\ R_{21} & V_{22}e^{-i(\delta_{21}+\delta_{12})} & V_{23}e^{-i(\delta_{21}+\delta_{12})} \\ R_{31} & V_{32}e^{-i(\delta_{31}+\delta_{13})} & V_{33}e^{-i(\delta_{31}+\delta_{13})} \end{pmatrix} \begin{pmatrix} d \\ se^{i\delta_{12}} \\ be^{i\delta_{13}} \end{pmatrix}. \quad (2.10)$$

The quark field redefinitions made above have no physical consequences, so we reduced the number of physically relevant real parameters from nine to four. These are three mixing angles and the CP violating complex phase. The CKM matrix in

$$\mathcal{L}_{CC}^{quark} = \frac{g}{\sqrt{2}} \left(\bar{u}, \bar{c}, \bar{t}\right) \gamma^{\mu}(1-\gamma_5)\mathbf{V} \begin{pmatrix} d \\ s \\ b \end{pmatrix} W_{\mu}^{+} + h.c. \quad (2.11)$$

is

$$\begin{pmatrix} V_{ud} & V_{us} & V_{ub} \\ V_{cd} & V_{cs} & V_{cb} \\ V_{td} & V_{ts} & V_{tb} \end{pmatrix} \quad (2.12)$$

The standard choice of parametrization is [8]

$$\mathbf{V} = \begin{pmatrix} 1 & 0 & 0 \\ 0 & c_{23} & s_{23} \\ 0 & -s_{23} & c_{23} \end{pmatrix} \begin{pmatrix} c_{13} & 0 & s_{13}e^{-i\delta} \\ 0 & 1 & 0 \\ -s_{13}e^{-i\delta} & 0 & c_{13} \end{pmatrix} \begin{pmatrix} c_{12} & s_{12} & 0 \\ -s_{12} & c_{12} & 0 \\ 0 & 0 & 1 \end{pmatrix} =$$
$$\begin{pmatrix} c_{12}c_{13} & s_{12}c_{13} & s_{13}e^{-i\delta} \\ -s_{12}c_{23} - c_{12}s_{23}s_{13}e^{-i\delta} & c_{12}c_{23} - s_{12}s_{23}s_{13}e^{-i\delta} & s_{23}c_{13} \\ s_{12}s_{23} - c_{12}c_{23}s_{13}e^{-i\delta} & -c_{12}s_{23} - s_{12}c_{23}s_{13}e^{-i\delta} & c_{23}c_{13} \end{pmatrix}, \quad (2.13)$$

where $s_{ij} = \sin\theta_{ij}, c_{ij} = \cos\theta_{ij}$ and δ is the mentioned phase responsible for all CP-violating phenomena in flavour changing processes in the Standard Model. It is convenient to rewrite the CKM matrix into the Wolfstein parametrization. We define [11]

$$s_{12} = \lambda = \frac{|V_{us}|}{\sqrt{|V_{ud}|^2|V_{us}|^2}}, \qquad s_{23} = A\lambda^2 = \lambda \left|\frac{V_{cb}}{V_{us}}\right|,$$
$$s_{13}e^{i\delta} = V_{ub}^{*} = A\lambda^3(\rho + i\eta) = \frac{A\lambda^3(\bar{\rho} + i\bar{\eta})\sqrt{1 - A^2\lambda^4}}{\sqrt{1-\lambda^2}\left[1 - A^2\lambda^4(\bar{\rho} + i\bar{\eta})\right]} \quad (2.14)$$

and the CKM matrix becomes

$$\mathbf{V} = \begin{pmatrix} 1-\lambda^2/2 & \lambda & A\lambda^3(\rho - i\eta) \\ -\lambda & 1-\lambda^2/2 & A\lambda^2 \\ A\lambda^3(1-\rho-i\eta) & -A\lambda^2 & 1 \end{pmatrix} + \mathcal{O}(\lambda^4). \tag{2.15}$$

The precise determinantion of the CKM coefficients is important, for they are fundamental parameters of SM. Numerical values of the CKM coefficients are [11]

$$\begin{pmatrix} 0,97428 \pm 0,00015 & 0,2253 \pm 0,0007 & 0,00347^{+0,00016}_{-0,00012} \\ 0,2252 \pm 0,0007 & 0,97345^{+0,00015}_{-0,00016} & 0,0410^{+0,0011}_{-0,0007} \\ 0,00862^{+0,00026}_{-0,00020} & 0,0403^{+0,0011}_{-0,0007} & 0,999152^{+0,000030}_{-0,000045} \end{pmatrix} \tag{2.16}$$

for Wolfenstein parameters they are

$$\begin{aligned} \lambda &= 0,2246 \pm 0,0011 & A &= 0,832 \pm 0,017 \\ \bar{\rho} &= 0,130 \pm 0,018 & \bar{\eta} &= 0,350 \pm 0,013 \end{aligned} \tag{2.17}$$

and for the Jarlskog invariant it is

$$J = (2,91^{+0,19}_{-0,11}) \times 10^{-5}. \tag{2.18}$$

2.3 Unitary Triangle

The unitarity of the CKM matrix imposes equations

$$\sum_i V_{ij}V_{ik}^* = \delta_{jk} \qquad \text{and} \qquad \sum_j V_{ij}V_{kj}^* = \delta_{ik} \tag{2.19}$$

These conditions, which lead to vanishing six combinations, can be represented as triangles in complex plane. The areas of the triangles are always same and equal to the half of Jarlskog invariant J, which is a phase-convention-independent measure of CP violation, defined by

$$Im\left[V_{ij}V_{kl}V_{il}^*V_{kj}^*\right] = J\sum_{m,n}\varepsilon_{ikm}\varepsilon_{jln}. \tag{2.20}$$

In Figure 2.2 we can see the most commonly used unitarity triangle arising from

$$V_{ud}V_{ub}^* + V_{cd}V_{cb}^* + V_{td}V_{tb}^* = 0 \tag{2.21}$$

which has, due to dividing each side by best-known coefficients $V_{cd}V_{cb}^*$, vertices (0,0), (0,1) and, in Wolfenstein parametrization, $(\bar{\rho}, \bar{\eta})$.

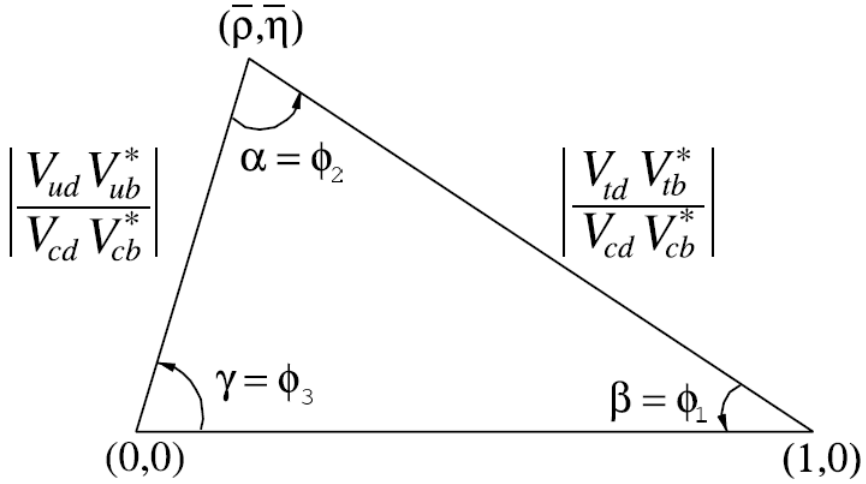

Figure 2.2: Sketch of the most commonly used unitarity triangle.[11]

Processes dominated by loop contributions in the SM, such as penguin decays, are very sensitive to new physics beyond the SM. They can be used to exctract CKM elements only if the SM is assumed. The penguin decays are provided by measurements of $\sin 2\beta$, which is very sensitive to the new physics. Besides the NA62 experiment, also $BABAR$ and Belle have measured the contribution of higher order amplitudes performed by penguin-dominated decays. From these two experiments the world average is [12]

$$\sin 2\beta = 0,6723 \pm 0,023.$$

In Figure 2.3 we can see the constraints on the $\bar{\rho}, \bar{\eta}$ plane from various measurements and the global fit result, where Δm_d and Δm_s are the mass difference between two neutral B and B_S^0 meson mass eigenstates, and ϵ_K is from measurement of CP violation in $K^0 - \bar{K}^0$ mixing. The goal of the NA62 experiment will be the measurement of coefficient $|V_{td}|$ with accuracy better than 10%. This coefficient with $|V_{ts}|$ coefficient cannot be measured from three-level decays of the top quark, so we have to measure them from $B - \bar{B}$ oscillations mediated by box feynman diagrams with top quarks, or loop-mediated rare K and B decays. To suppress theoretical uncertainties in hadronic effects limit, we are taking the ratios of processes that are equal in the flavor $SU(3)$ limit to determine $|V_{td}/V_{ts}|$. In the NA62 we focus on the rare kaon decay $K^+ \to \nu\bar{\nu}$, from which a theoretically clean determination of $|V_{td}V_{ts}^*|$ is possible. Experimentally, only seven events have been observed [13] and the rate is consistent with the SM with large uncertainties. Much more data is needed for a precise measurement and that is the aim of the NA62.

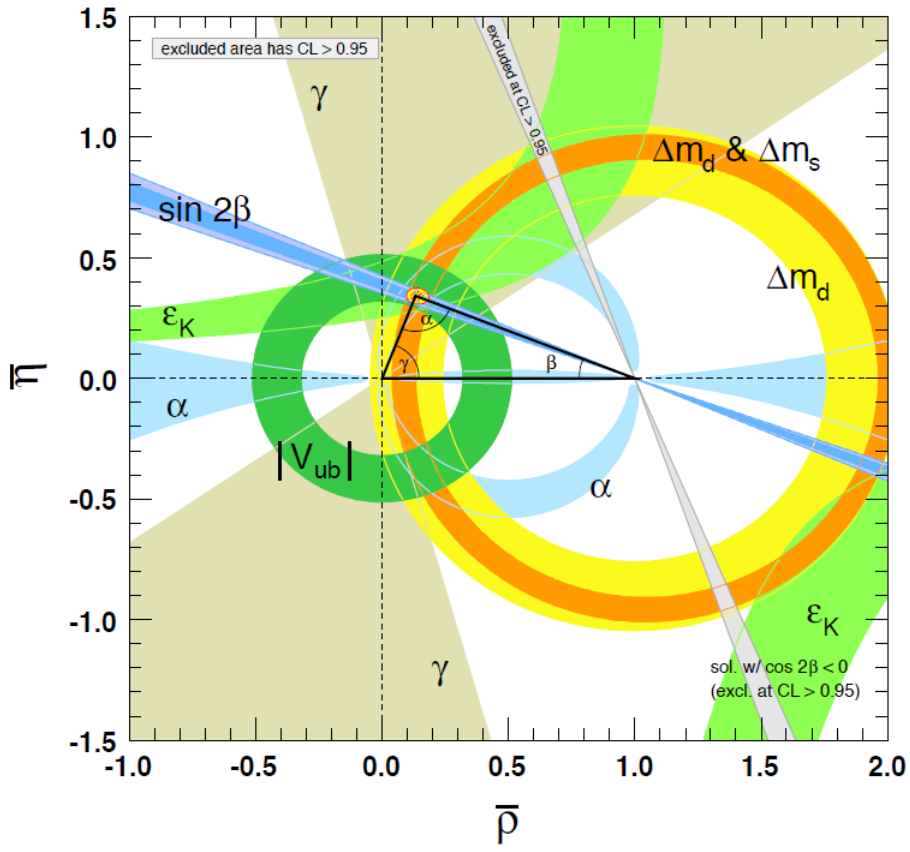

Figure 2.3: Constraints on the $\bar{\rho}, \bar{\eta}$ plane with shaded area of 95% CL.[11]

At the quark level the two processes arise from the $s \to d\nu\bar{\nu}$ process. In Figure 2.4 we can see two processes, which in the SM originate from a combination of the Z^0 penguin, on the left and a double W exchange on the right. In these graphs the u, c, t quarks appear as internal lines and the hard GIM mechanism implies that the top-quark contribution dominates.

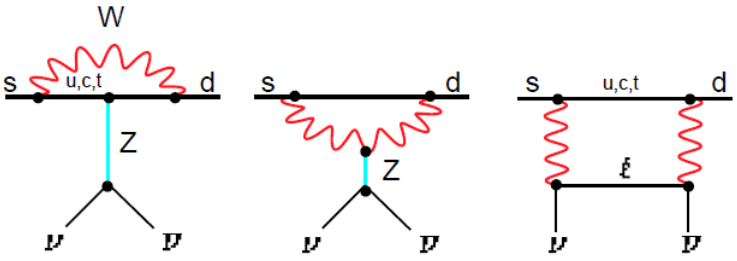

Figure 2.4: Graphs for $s \to d\nu\nu$ in SM.[14]

On the other hand, new effects in SUSY models can be for example induced through new box and penguin diagram contributions, which involve new particles such as charged Higgs or charginos and stops that replace the W boson and the up-type quark of the SM, as we can see in Figure 2.5.

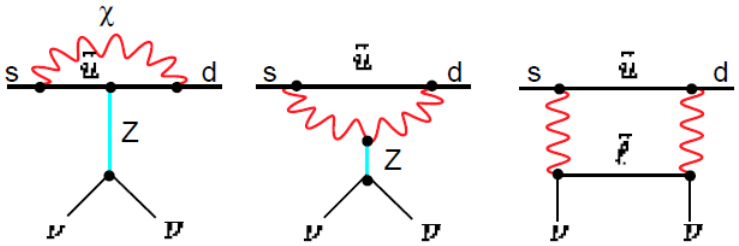

Figure 2.5: Graphs for $s \to d\nu\nu$ in SUSY.[14]

2.4 Other physics opportunities

Besides the main aim of the experiment described above, the apparature of NA62 has good energy resolution for photons and that allows us to study the radiative kaon decays with unprecedented precision. In recent times, most important hadronic K decay results were obtained from dedicated precision experiments, not as byproducts of experiments designed for something else, so to extract all experimental potential of this apparature many other kaon decays are planned for testing different physical theories. Particulary we are talking about investigating CP violation and Chiral Perturbation Theory (ChPT). On the NA62 would be in the second phase also K_L flux with intensity 5-10 times grater than on NA48 experiment and after SPS upgrade it could be 100 times more. That is great potential for other rare decays [15].

An accurate value of CKM coefficient V_{us} is crucial in determinantions of the other parameters and in tests of CKM unitarity. To obtain the V_{us} of precision comparable to that obtained in kaon decays, we would like to see improved data particulary in $\Xi^- \to \Lambda e^- \bar{\nu}_e$, which could be done on the NA62 experiment [16].

2.4.1 Other searches for New Physics in rare kaon decays

It is necesary to use different modes to disentagle SM from new physics and long-distance from short-distance. Another models with non-MFV witch have besides the exeptionally clean mode $K^+ \to \pi^+ \nu\bar{\nu}$ large effects are also

$$K_L \to \pi^0 \nu\bar{\nu}, (BR \sim 10^{-8}),$$

$$K_L \to \pi^0 e^+ e^-, (BR \sim 10^{-10}),$$

$$K_L \to \pi^0 \mu^- \mu^+, (BR \sim 10^{-10}),$$

which can be improved by experiment and have different sensitivity to new physics, and

$$K_L \to \mu^- \mu^+ (BR \sim 10^{-9}),$$

$$K_L \to e^- e^+ (BR \sim 10^{-12}),$$

which can be improved by theory. Some of these contributions are potentially correlated and there might be constraints from ε_K and ε'/ε. Since

$$K_L \to \pi^0 l^+ l^- \ (l \text{ is for lepton})$$

modes are well under control, the detection of

$$K_L \to l^+ l^-$$

is more difficult [17]. Backrounds of

$$K_l \to e^+ e^-$$

are

$K_L \to ee\gamma$, $(BR \sim 10^{-6})$, $ee\gamma\gamma$, $(BR \sim 10^{-7})$, $eeee$, $(BR \sim 10^{-8})$, with lost particles,

$$K_L \to \gamma\gamma, (BR \sim 10^{-4}), \text{with conversions}$$

and

$$K_L \to \pi e\nu, (BR \sim 10^{-2}).$$

Backrounds of

$$K_L \to \mu^- \mu^+$$

are

$$K_L \to \pi\mu\nu, (BR \sim 10^{-2}), \text{ with pion decay}$$

and

$$K_L \to \pi e\nu, (BR \sim 10^{-2})$$

with pion decay and electron mis-ID [15]. There would be also measurement of

$$K_L \to \pi^0\pi^0, \, (BR \sim 10^{-4})$$

like on NA48 experiment, but with better resolution thanks to LAV. The NA62 can also measure radiative decays like

$$K_S \to \pi^0 l^+ l^-, \, (BR \sim 10^{-9}),$$

$$K^+ \to \pi^+ l^+ l^-, \, (BR \sim 10^{-7}),$$

$$K \to (n\pi)\gamma\gamma,$$

$$K \to (n\pi)\gamma$$

which are FCNC, but have very different loop functions [18].

2.4.2 Investigation of direct CP violation

In kaon decays we can also study direct or indirect CP violations in modes like

$$K^+ \to \pi^+ l^+ l^-$$

or

$$K^+ \to \pi^+\pi^0\gamma, \, (BR \sim 10^{-6})$$

and more, which are sensitive to different conditions and also could test SM. For example direct CP asymmetry

$$A_{CP} = \frac{\Gamma(K^+ \to \pi^+ l^+ l^-) - \Gamma(K^- \to \pi^- l^+ l^-)}{\Gamma(K^+ \to \pi^+ l^+ l^-) + \Gamma(K^- \to \pi^- l^+ l^-)}$$

is sensitive to interference between the up γ penguin and charm, top contributions. It is expected to be in the 10^{-5} range in the SM. Direct CP asymmetry

$$A_{CP} = \frac{\Gamma(K^+ \to \pi^+\pi^0\gamma) - \Gamma(K^- \to \pi^-\pi^0\gamma)}{\Gamma(K^+ \to \pi^+\pi^0\gamma) + \Gamma(K^- \to \pi^-\pi^0\gamma)}$$

is sensitive to electromagnetic operator and the value is again expected to be small in the SM (10^{-5}). Mode

$$K_L \to \pi^0 l^+ l^-$$

is richer since it probes also the Higgs penguins [18].

Other kaon CP violating modes are:

$$K^+ \to \pi^+\pi^0\gamma\gamma,$$

$$K^+ \to \pi^+ e^+ e^- \gamma,$$

$$K^+ \to \pi^+ \pi^0 \gamma$$

[21]. CP violation has been also measured in

$$K_L \to \pi^+ \pi^- e^+ e^-,$$

with similar muon mode, but that has BR in the 10^{-14} range [18].

$K^\pm \to \pi^\pm \pi^0 \gamma$ - assuming 10^{13} K^+ K^- beam flux (no downscale), we can measure rate assymetry down to 10^{-4} precision. We can also measure Dalitz plot asymmetry T_π^* and W. The measurement of the ϕ angle in the interference term can be done, too. K^+/K^- ratio measurement can use $\pi^\pm\pi^0$ normalization and systematics can be pushed down to 10^{-4} by using 4 ratio as for $\pi^\pm\pi^0\pi^0$ [19].

$K^\pm \to \pi^\pm \gamma\gamma$ - Present PDG have no limit on asymmetry. The NA62 might get 850 000 K^+ and 303 000 K^-. There is no evidence of systematic limit on the measurement and NA62 can push the assymetry limit down to 10^{-3} [19].

$K^\pm \to \pi^\pm e^+ e^-$ and $K^\pm \to \pi^\pm \mu^+ \mu^-$ - NA48/2 reached a limit of $2,1 \times 10^{-2}$ at 90% CL. The NA62 might collect 450 000 K^+ and 250 000 K^-, what can reduce present limit of CP violation by 1 order of magnitude. The SUSY upper limit is on the range of 10^{-3}. On this decay we can also measure forward-backward asymmetry [19].

Non-leptonic kaon decays is another possibility to measure direct CP violation and have experimentally well established value: $Re\left(\frac{\varepsilon'_K}{\varepsilon_K}\right) = (1,64 \pm 0,20) \cdot 10^{-3}$. These decays can either confirm or show deviations of the SM. They can also help to understand strong-weak dynamics interplay. Decays from this section are:

$$K \to \pi\pi, \; (BR \sim 10^{-2}),$$

$$K^+ \to \pi^+ \pi^0 \pi^0, \; (BR \sim 10^{-2}),$$

$$K^+ \to \pi^+ \pi^+ \pi^-, \; (BR \sim 10^{-2}), \text{ etc.}$$

Especially $K^+ \to 3\pi$ vs. ε'_K violating charge assymeties are interesting to decrease present experimental uncertainity. It is also important to help in finding-constraining new physics and understanding analytically ε'_K [20].

2.4.3 Investigation of Chiral Perturbation Theory (ChPT)

ChPT is the effective field theory of the SM at low energies and describes interaction between pions, kaons, photons, ..., and it tries to match QCD in the non-perturbative regime. When considering the most general Lagrangian with symmetries and relevant degrees of freedom up to given order, one has to deal with many a priori unknown couplings. The way to solve this issue is to relate different decays with same unknowns, what is with the long list of works applying ChPT to kaon decays with many new modes, ideal field for investigation of NA62 [20]. This section obtains decays for chiral test like

$$K \to \pi\pi\gamma, \ (BR \sim 10^{-6}),$$

$$K \to \pi\pi e^+ e^-, \ (BR \sim 10^{-5}),$$

or

$$K_{L,S} \to \pi^0\pi^0\gamma\gamma, \ (BR \sim 10^{-9}),$$

$$K_S \to \gamma\gamma, \ (BR \sim 10^{-6}),$$

$$K_L \to \pi^0\pi^{0"}\pi^{0"} \to \pi^0\pi^0\gamma\gamma$$

[21]. With BR$\sim$ 21% the decay

$$K^+ \to pi^+ pi^0$$

represents an important source of neutral pions. This can be used for further studies of properties of the lightest meson π^0. As an example one can name decays:

$$\pi^0 \to e^+e^-\gamma$$

or

$$\pi^0 \to e^+e^-$$

which can be a potential of new physics as there exists already a discrepancy between experiment and theory (see [22]). All branching ratios in this chapter are from [4].

2.4.4 Conclusion

To satisfy these compelling aims, the whole system of detectors is needed. The schematic view of them is in Figure 2.6, and descriptions are in following chapters.

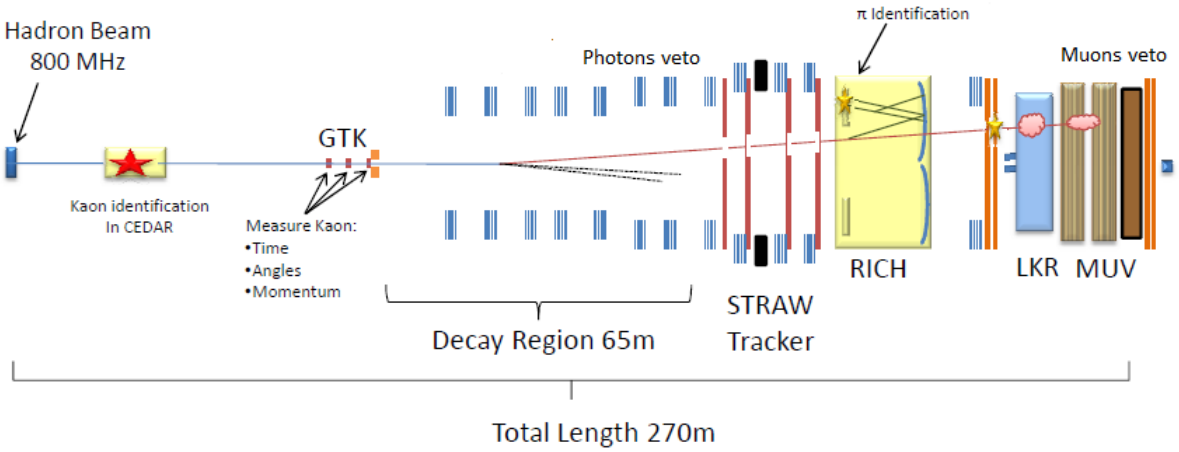

Figure 2.6: Conceptual layout of NA62 experiment [23]

3. A Differential Cherenkov counter CEDAR and KTAG

3.1 Introduction

Positive kaons in the beam can be tagged positively by using an upgraded version of the existing CEDAR differential Cerenkov counters [24]. The CEDAR counters are two SPS detectors for high energies (North CEDAR) and for low energies (West CEDAR). For us the ideal solution is a West CEDAR filled with hydrogen gas, to significantly reduce the scattering of the beam in the gas. In Figure 3.1 the general optical layout is shown. By reducing the diaphragm aperture around the passage of photons from K^+ only, the light from pions and protons is blocked. To manage rates about 50MHz we have to add the KTAG (kaon tag) to support CEDAR and replace old photomultipliers for individual 10 mm photomultipliers, 64 per octant [25]. The design of the KTAG and its lightguide is the key to ensure maximum light collection and so reliable kaon tagging. In Figure 3.1 we can see both, CEDAR and KTAG.

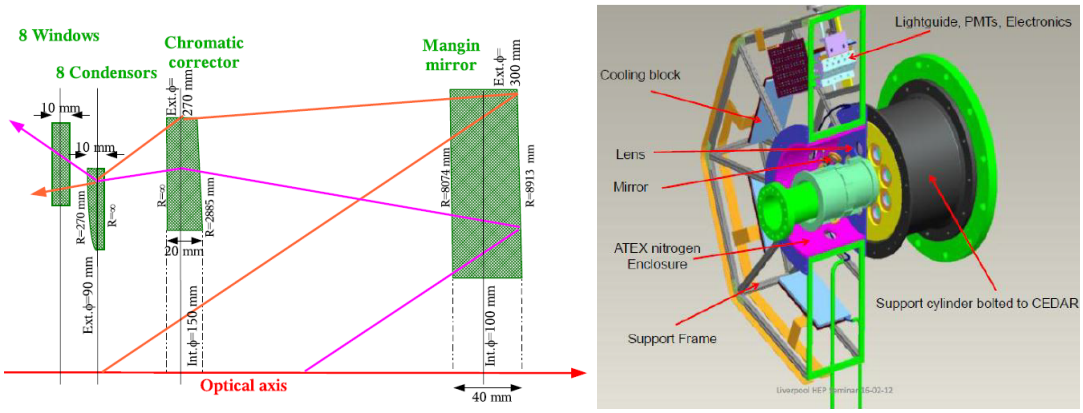

Figure 3.1: View of the CEDAR optics (left)[14] and KTAG model with connection to CEDAR (right)[25].

4. GIGATRACKER

4.1 Introduction

The GigaTracKer (GTK) is a spectrometer that provides precise measurements of momentum, time and angle of the incoming 75 GeV/c kaon beam. This measurement is essential to select $K^+ \to \pi^+ \nu\bar{\nu}$ decay. The background reduction will be achieved by the kinematical constraint based on the missing mass variable:

$$m^2_{miss} \approx m^2_K \left(1 - \frac{|P_\pi|}{|P_K|}\right) + m^2_\pi \left(1 - \frac{|P_K|}{|P_\pi|}\right) - |P_K||P_\pi|\Theta^2_{\pi K} \quad ,$$

where $|P_K|$ is derived from GTK, $\Theta^2_{\pi K}$ from both GTK and STRAW Tracker, and $|P_\pi|$ from STRAW Tracker. The Gigatracker is composed of three silicon pixel stations (GTK1, GTK2 and GTK3) mounted around four achromat magnets as shown in Figure 4.1 [3]. The GTK is placed in vacuum along the beam line, just before the fiducial area.

4.2 Specification

The GTK has to measure momentum with the relative resolution of 0,2% and direction with precision of the order 16 μrad. The pixel size of 300 μm x 300 μm, with 200 μm thickness (0,5% X_0), is sufficient to achieve the required precision. Totally, each station is made of one hybrid silicon pixel detector with the total size of 63.1 mm x 29.3 mm containing 18000 300 μm x 300 μm pixels arranged

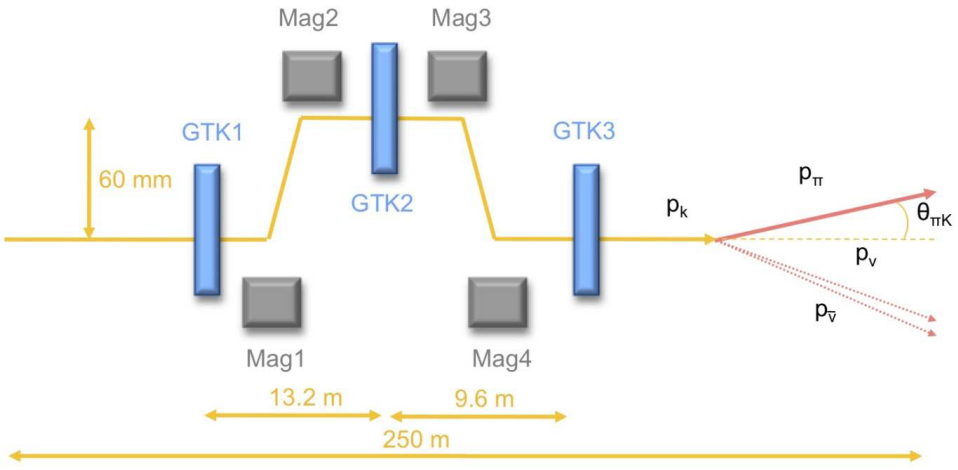

Figure 4.1: View of the beam illustation in GTK layout.[3]

in the matrix of 90 x 200 elements. With this configuration the detector matches the expected beam dimensions of $\sim$ 60 mm x 27 mm. The hit arrival time of a pixel cell is measured with the precision of at least 200 ps in each station, what gives us a overall time resolution better than 150 ps.

To reduce the radiation induced current leakage, the operating temperature is set to maximum 5°C, however efforts are being made to design the cooling system to operate at -20°C, which allows the operation of 100 days. The baseline choice for a sensor material is p-in-n due to simpler processing procedures, availability and experimental arrangement [3].

4.3 DAQ

In order to minimize the radiation lenght of the GTK and maximize geometric efficiency in the active beam area any connections to the read-out chip are outside the beam area. The read-out is covered by application specific integrated circuits (ASIC), which are creating the front-end chips and On-detector readout. Each pixel cell contains one bump pad to connect it with the corresponding cell in the front-end chip.

Then there is the off detector readout system, which aim is to provide the interface to the on detector electronics, the DAQ system, the trigger system and the NA62/GTK detector control system (DCS). The off-detector electronics must receive the data pushed by the on-detector GTK ASICs, save it on the temporary buffers for the L0 trigger latency time, select the GTK data matching the L0 trigger request and send packets of events to the sub-detector PCs [3].

5. Charged Anticounters (CHANTI)

5.1 Introduction

The sets of square anticounters are situated after the last Gigatracker station in order to reduce a critical background induced by inelastic interactions of the beam with the collimator and the Gigatracker (GTK) stations. The CHANTI also have to tag beam halo muons in the region close to the beam. Although the CHANTI is not at L0 trigger level, due to rate about 2 MHz it has to have time resolution better than 2 ns. Six small squares have side length 300 mm with a rectangular hole in the middle for the beam (50 mm in y and 90 mm in x axis). Each station is made from two layers, called the layer x and y respectively. The y(x) layer is composed of 22 (24) scintillator bars arranged parallel to the x(y) direction and individually shaped at appropriate length (with respect to the hole in the middle). Each layer is in the end composed by two sublayers, made up by 10+12 (10+14) bars, and staggered by half bar. Each bar is triangularly shaped, and two staggered bars face oppositely. The collected light is distributed from each scintillator bar via the WLS fibre and detected by photomultiplier on one side [3].

6. Large Angle Veto (LAV)

6.1 Introduction

To suppress the dominant background originating from the decay $K \to \pi^+\pi^0$ (BR=20.7%) to the specified level, photon vetoes detector: Large Angle Veto (LAV) has been made. This detector covers the angular region between 8,5 mr and 50 mr. To detect angular region between 1 mr and 8,5 mr is the LKR used and around the zero angle is operating the SAC and IRC. With such a configuration, the average inefficiency for the rejection of the π^0 should be smaller than 10^{-8} and only about 0.2 % of the $K \to \pi^+\pi^0$ events have one photon from the π^0 left undetected. The LAV is composed of 12 stations situated between 120 and 240 m from the target along the beam axis. The first eleven stations are the part of vacuum decay tube, while the last one is located outside the vacuum tank. The LAV stations have a diameter going from 2,1 on the downstream end to 3 m upstream. The basic building blocks of these detectors are lead glass crystals with attached photomultipliers (PMT) from the former OPAL electromagnetic calorimeter [3]. Each lead glass block from the former OPAL experiment has the shape of truncated prism of Schott SF57 lead glass [27]. Four blocks (lead glass crystals + PMT's) are mounted on a common support structure forming an azimuthal segment (Figure 6.1). Inside the vacuum tube the azimuthal segments are assembled forming a complete ring of lead glass blocks. First eight LAV stations are made from 5 and the last four from 4 rings, which are staggered in the azimuth to provide the complete hermeticity of at least three blocks in the longitudinal direction [26]. Each vessel is supported by four feet located at 30 degrees from the vertical axis of the cylinder, as we can see in Figure 6.1.

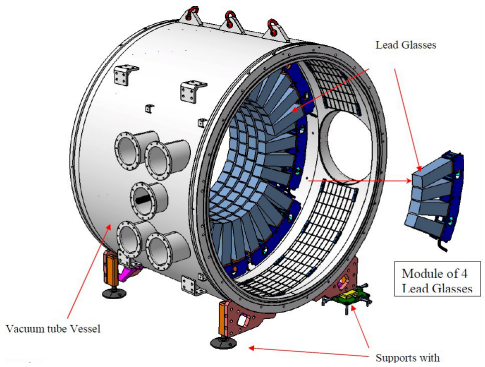

Figure 6.1: Complete station layout.[23]

7. Straw tracker

7.1 Introduction

As the most promising detector operating in the vacuum a Straw Tracker has been chosen. The architecture of the Straw Tracker is based on the experiences of COMPASS and ATLAS experiments. The purpose of the Straw Tracker is to measure the direction and the momentum of secondary charged particles originating from the decay region with a good accuracy. The whole detector consists of four chambers and each of them is equipped with 1792 straw tubes. The straws in the chamber are orientated in four directions as we can see in figure 7.1. In the

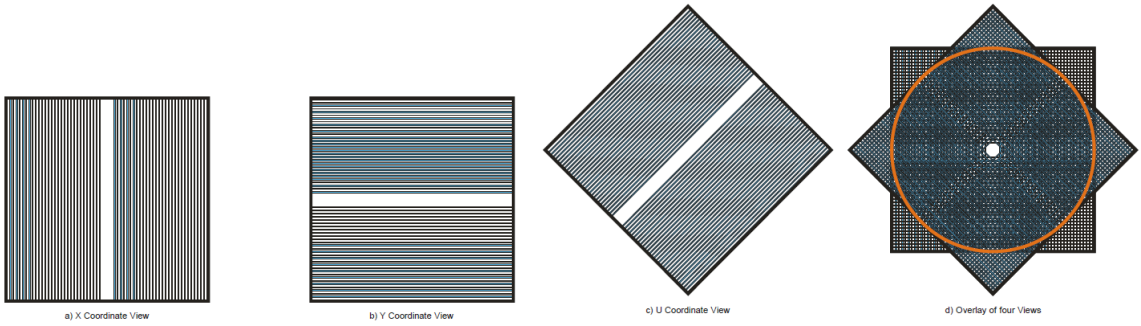

Figure 7.1: Schematic drawing of four views of the each chamber of Straw Tracker. We can also see the central gap.[3].

middle of each direction part of the chamber is approximately 12 cm thick central gap because of location of the beam pipe, as we can see also in figure 7.1. The chambers are intercepted in the middle by a high aperture dipole magnet providing a vertical B-field of 0,36T (see figure 7.2), which deflects the beam up in the vertical direction. Because of that the 3^{rd} and the 4^{th} chamber are shifted from the direct beam axis to the position of deflected beam. The straws are 210cm long and consist of tube which acts like a cathode and a wire which acts like an anode. The tubes are made of ultra-light 36μm thin PET foils coated inside with with 0,05μm thin Cu layer and 0,02μm Au layer. These metals provide the conductance of inside part of the tube. Firstly we have only the PET foil with the appropriate dimensions on which is accomplished coating with the mentioned metals by sputtering process.. After that are rolled into the cylinder and by ultrasonic welding seamed to create the tube with diameter 9,8mm without any

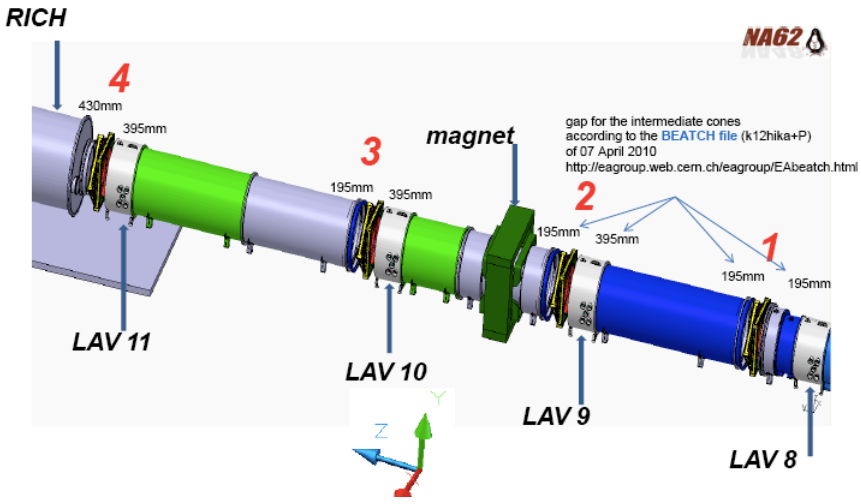

Figure 7.2: Schematic view of Straw Tracker in the experiment. The beam direction is along positive z-axis. The chambers are marked with red numbers 1,2,3 and 4.[3].

overpressure. Several gas leakage and tension tests have to be done on the tube to verify the seam.

After manufacturing the tubes in Dubna, they are overpressured and moved to CERN, where another tests are made. A After that are equipped by $\varnothing = 30\mu$m wire, which is made of gold-plated tungsten, and assembled into the straw chambers. In the straw is a gas mixture $ArCO_2$ (fast gas) in ratio 70:30. When the particle hits the straw, it starts drifting through and ionizing the gas. Between the tube and the wire is a high voltage 1650V and current threshold on the wire is 2fC, so when the particle creates more charge, it can be detected.

7.2 Straw in the chamber and DAQ

The straws in the chamber have two sides:a near end and a far end. On the near end are Webs, gas supply, wiring of the straws and Cariocas (see Figure 7.3). Each sixteen straws have own Web and manifold as we can also see in figure 7.3. On the far end are resistors used to avoid the signal reflections which can deteriorate the signal especially at high rates.

The geometry of the straws in the chamber is shown in Figure 7.4. There are 112 straws in each layer and the distance between the straws in one layer is 17,6 mm. This distance is with respect to the condition, that straws can not touch each other and due to different pressure outside and inside the straw, they are inflated. To conserve the distance between the straws, we use two spacers. This

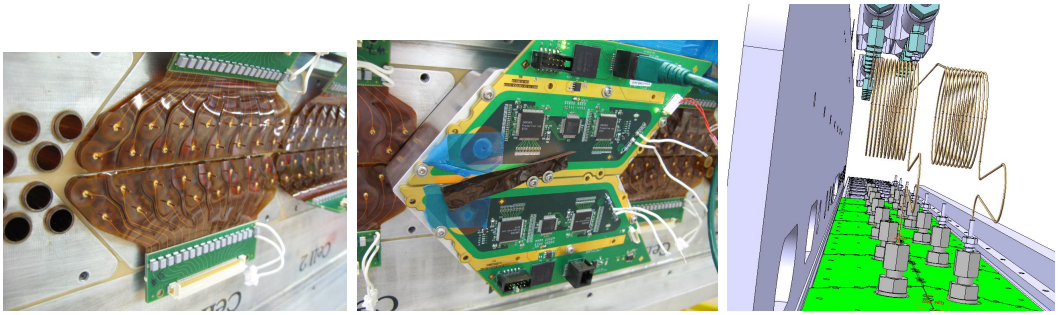

Figure 7.3: Front-end electronics (Webs on the left and Cariocas in the middle) and gas manifold (on the right).[28]

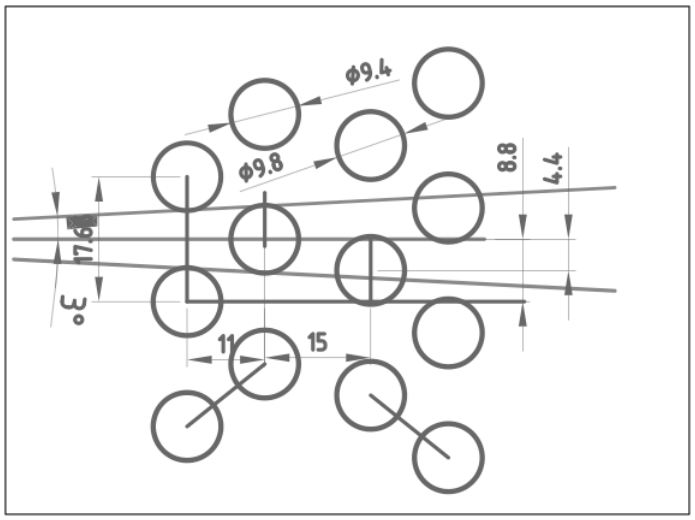

Figure 7.4: Straw layout in one view (beam direction from left to right). The distance between the straws in one layer is 17,6 mm.[3]

geometry with four layers is used because near the wire we get a bad resolution and on the other hand near the edge is the best resolution. This geometry also guarantee at least two hits per view and avoid a signal gap. The layers are shifted against each other to solve the right-left ambiguity. It can be shown that the decay products $\pi^+\pi^0$ and $\pi^+\pi^0\pi^0$ from $K^+ \approx 75$GeV are deflected from the beam axis with maximum angle 3 degrees.

For DAQ we use on-detector electronics consists of an 8-channel analogue front-end chip Carioca, developed for the LHCb muon chambers, containing a fast preamplifier, semi-gaussian shaper, a tail cancellation circuitry, base line restorer and a discriminator. After that the signal goes to a TDC (time to digital converter), which converts sporadic pulses to the digital time representation. The output of TDC is the time of arrival and the end of each incoming pulse. For the

TDC magnitudes are not important. Detectors detect the risings and fallings of edges. When it happens the values of the counters are saved in the corresponding registers.

7.3 Requirements and their solutions

A spatial resolution of this detector better than 130μm per coordinate and better than 80μm per space point is needed. An ultra-light material for the tube shall be used, in order to the radiation length would be better than 0,5% for each chamber. Than we need to achieve reliably operation in a high rate environment, because near the beam the rate is up to 0,5MHz per straw. Finally this detector has to contribute as multiplicity veto to the trigger. The last requirement has been tested via Monte Carlo simulation of the possible background decays. With the overall inefficiency level of 5% the three-track veto efficiency is not significantly changed and decays like $K \to 3\pi^{+-}$ and $K \to \pi^+\pi^-\mu^+\nu$ can be easily suppressed by spectometer multiplicity veto down to the level of 10^{-8}. On the other hand there occurs a problem with $K \to \pi^+\pi^-e^+\nu$ decay with low energy positron, because in this decay mode is a negative pion which leaves first three chambers and hits only one straw in the last chamber. But it is not so crucial with respect to the fact, that the negative pions hits the Jura side of the chamber, while the simulation shows the highest peak rates on the Saleve side. As a conclusion one can say that with the straw inefficiency of better than 5% background from $K \to \pi^+\pi^-e^+\nu$ will be suppressed and the maximum rate per straw can be estimated at the level of 0,5MHz [3].

7.4 Irradiation test of the straws and their components

The isotope of iron Fe^{55} which produces gamma photons with energy 5.9KeV has been used as a source for the irradiative test. It is a convenient radioactive source which is being used in aging tests, because it gives great energy deposition to the investigated material and it is not so harmful for people. All tests have been done by group of Serguei Konovalov at the irradiation facility in building number 155 at CERN and I have processed data into the report. The individual components of the straw and gas systems have been tested. The experimental sut-up to validate these components has been consisted of two pipes, for distribution the gas, and the measured component between them. The irradiation from the source has

been acting to the part of set-up through the window. Than the amplitude scan has been made [29]. The arrows in the graphs indicate direction of the gas flow and dashed rectangles define areas, which were irradiate. The parameters during the aging test are summarized in Table 1.

The plastic connector has been tested between two pipes mentioned above.

Gas mixture	Gas flow	Current	Irradiation area	High voltage	Fe^{55}-scan slit size
Ar(70%) CO_2 (30%)	0.5 cm^3/min	280 nA	20 mm	1725V	1 mm

Table 7.1: Parameters for the aging test-up

In the test there were two connectors in irradiation region. Result of the first

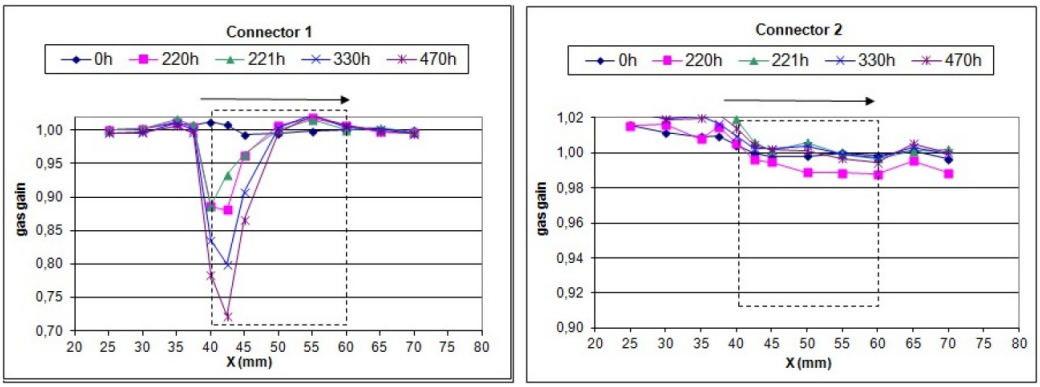

Figure 7.5: The first pipe with connector (left) and the second pipe with the connector (right)

measurement is shown in Figure 7.5 for the first and for the second connector. In the left figure, for the first connector, we can see obvious aging. So the test without the connector and with same pipes has been made to verificate the pipes. Results of measurement without connectors are shown in Figure 7.6.

In the first case there is obviously aging. As we can see from the comparison of graphs with and without connectors, not only the connector suffers from aging, but it can be also the pipe. It is indication of hydrocarbons from some organic compound or silicon dioxide. One additional measurement with the same connector but different pipe has been made. It finally validated the connector. The next measurement was the validation of the fittings, which are used in gas distribution system. The experimental configuration was the same, but now there were 3 samples. The reasults are shown in Figure 7.7. We can see that there is no aging of the fittings, so the validation is successful. In earlier measurements of ATLAS experiment it was found that silicon and organics compounds are very sensitive to

radiation. Its structure is damaged, silicon dioxides or hydrocarbons are created, and than it can bound electrons. These products are depositing on the wire and creates there an insulating layer. So electrons are captured by silicon dioxide or hydrocarbons instead of drifting through the straw, and we have no current and no signal. Even atomic layer can act like insulator, so it is very important to protect the straws from silicon and organics. It can appear on the straw from bad polymerized glue, or from lubricant that is used to smooth operating of bearings, which are used during the assembly. The prototype for validation of these components has been built. It is shown also with set-up in Figure 7.8. There are results given in Figure 7.9. We can see no aging in amplitude scans, so we can consider the prototype to be validated. Nowadays the pipe from gas distribution system is validating. In the future there will be some another irradiation tests of high voltage cables and cover. From previous experiments we know that the PCR don't have aging.

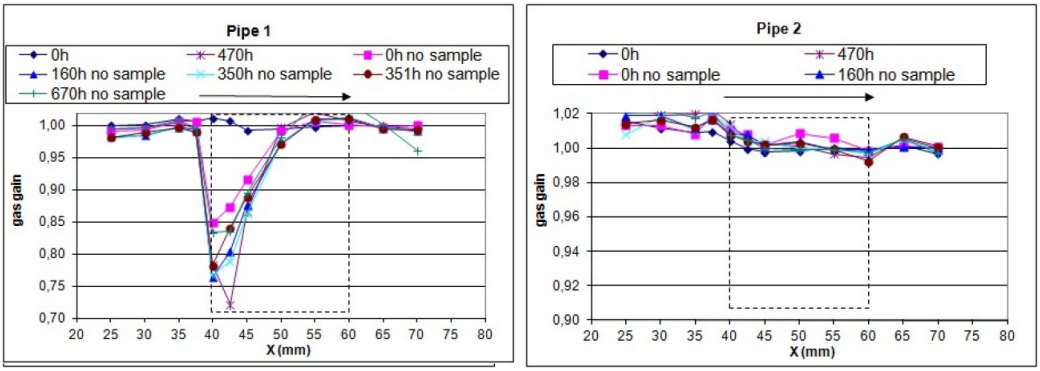

Figure 7.6: The first pipe without connector (left) and the second pipe without the connector (right). There is also one part from previous measurement with connector to comparison.

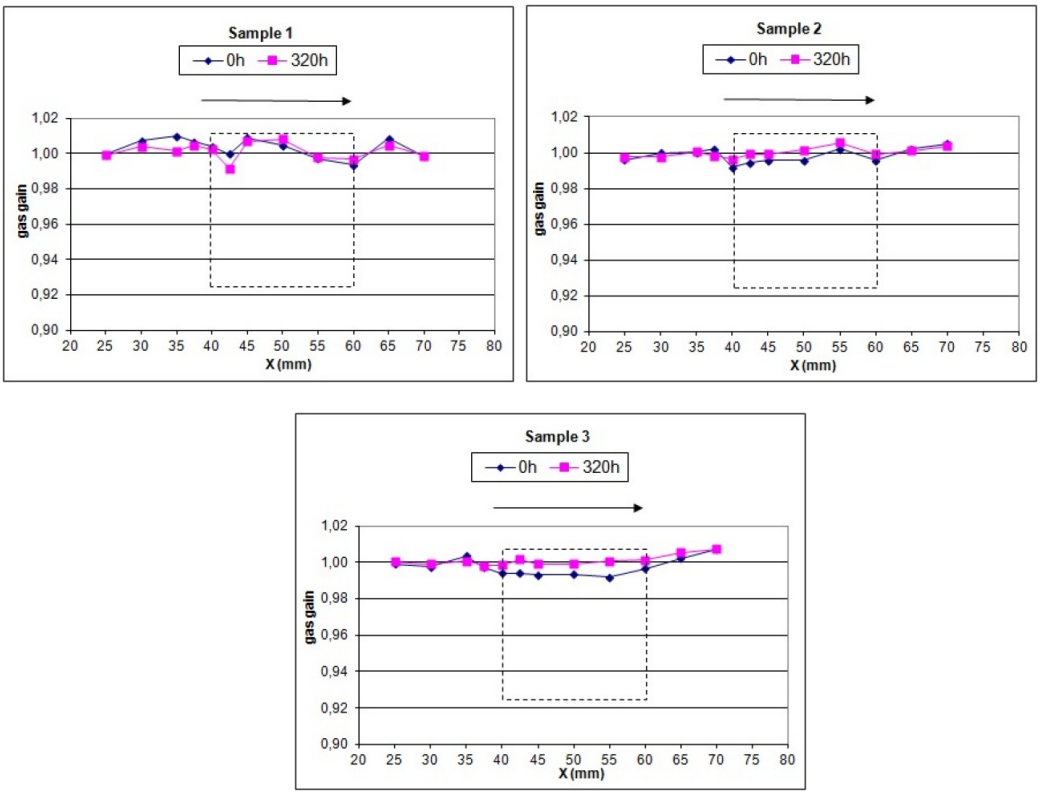

Figure 7.7: Validation of three fittings

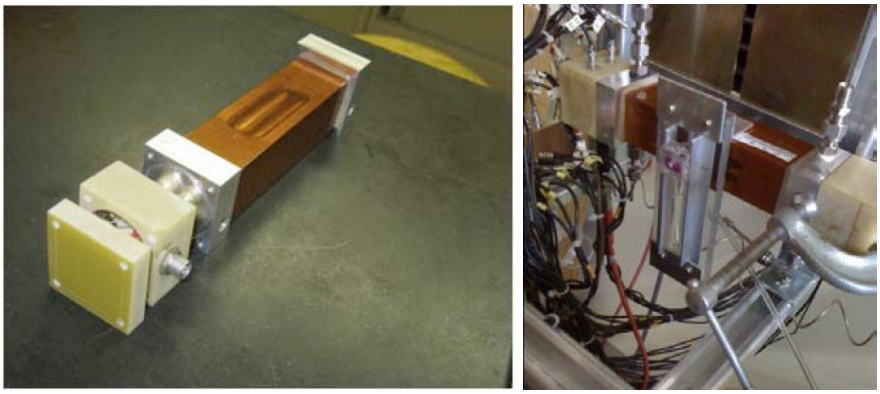

Figure 7.8: Straw prototype for material validation (left) and mounted in the set-up (right). [3]

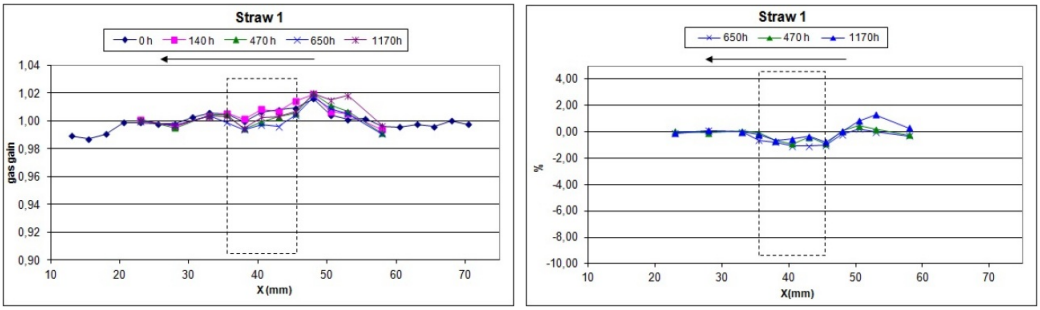

Figure 7.9: Amplitude scan along the straw (left) and it's normalization (right)

8. Ring Imaging Cherenkov counter (RICH)

8.1 Introduction

A Ring Imaging Cherenkov counter (RICH) is a detector used for particle identification. It consists of 18 m long vessel with diameter 3,8 m filled with a neon gas which has appropriate index of refraction. On the ends of the vessel are two spherical mirrors down the beam, and 2000 photomultipliers (PMTs) on the other end. Schematic view of RICH is in the Figure 8.1. Mirrors are reflecting a Cherenkov radiation to the opposite side of the vessel, where are the PMTs.

The Cherenkov radiation is an electomagnetic radiation, which is emitted when a charged particle is crossing through the medium with phase speed grater than the speed of light in that medium. The Cherenkov radiation is emitted at an angle Θ and creates a Cherenkov cone of half angle. This angle depends on the index of refraction of the medium n and the velocity β of the particle by known equation:

$$\cos\Theta = \frac{1}{\beta n}.$$

We need to separate μ^+ from π^+ between 15 and 35 GeV momentum providing a muon suppression factor at least 10^{-2}. To satisfy this condition we need to fill the vessel with neon at atmospheric pressure. Then we need to approach the time resolution of the crossing pions about 100 ps or better and produce a trigger for the charged tracks [3].

8.2 The Mirrors

To image the Cherenkov cone into a ring on its focal plane a mosaic of spherical mirrors is used, which is divided into two spherical surfaces to avoid an absorption of reflected light on the beam pipe. The mosaic consists of the matrix of 20 mirrors. 18 are hexagonal shape and two, near the beam pipe, are semi-hexagonal shape. The hexagonal shape mirrors are equipped with piezoelectric actuators, which allow remotely controlled orientation. Two mirrors near the beam are fixed in their position [3].

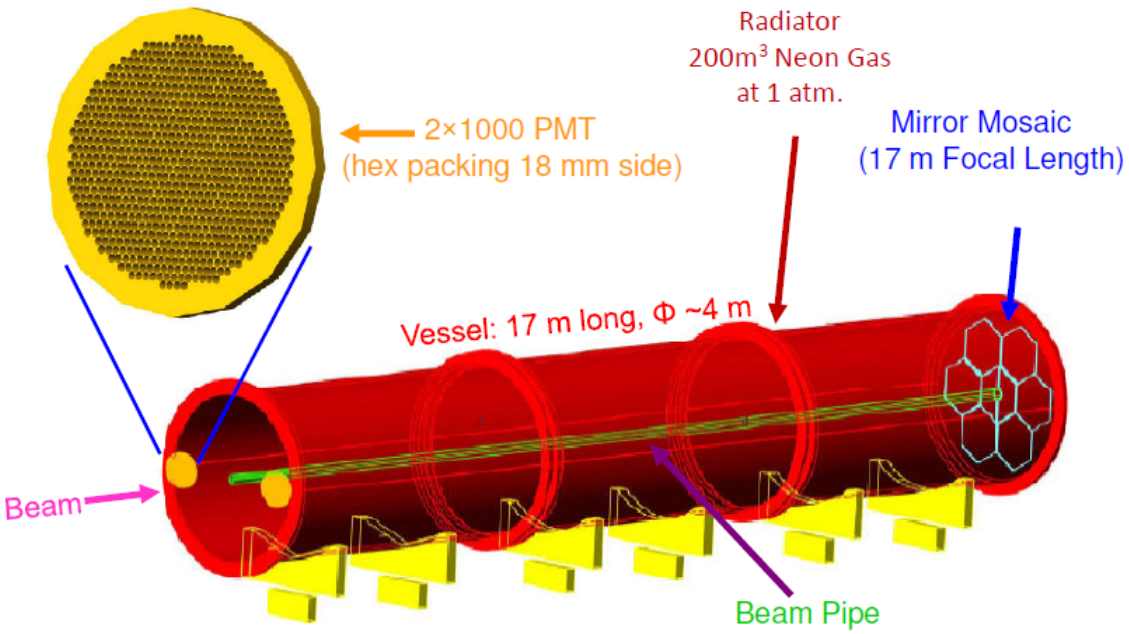

Figure 8.1: Schematic view of RICH. [23]

8.3 The Photomultipliers

From the requirements stated above, such as the time resolution and the trigger, we need a fast single anode PMTs, which size is as small as possible. Finally from the results of the 2007 Prototype Test Beam [30] has been extracted Hamamatsu R7400U-03 at 800 V as the most appropriate PMT, with respect to cost. This model with a UV glass entrance window cuts the sensitivity at 185 nm.

9. Small Angle Vetoes (IRC and SAC)

9.1 Introduction

The Intermediate Ring Calorimeter (IRC) is at the entrance of the LKR calorimeter and the Small Angle Calorimeter (SAC) and covers the zone near 0 degrees after the muon deflecting magnet. Both calorimeters are thick enough ($\approx 17X_0$) in order to keep the punch through probability below 10^{-7}. This solution will provide the photon detection inefficiencies of 10^{-6} or better at the high energies involved [14].

9.2 Geometry of the detectors

To build both detectors, IRC and SAC, the same technique has been used. This technique is known as "shashlyk technique": The calorimeter is made from 100 layers of 1 mm lead (more precisely 97% lead and 3% antimony alloy) and 2 mm scintillator. The thickness is approximately $17X_0$ and a fiber spacing is 9,5 mm [14]. It is made with a photomultiplier on the back as is shown in Figure 9.1.

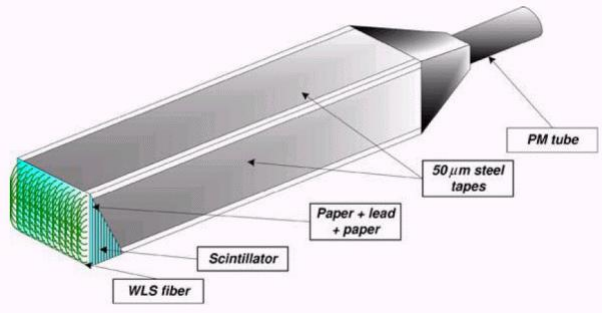

Figure 9.1: The concept of a shashlyk calorimeter.[14]

9.3 Readout

The readout of the small angle vetoes could follow the same scheme as the one for the large angle vetoes.

10. Charged Hodoscope (CHOD)

10.1 Introduction

A charged hodoscope is a detector, which serves as L0 trigger for charged particles back-up for RICH in the mirror plane. This detector is reused from NA48 experiment. It consists of 128 scintillators in two perpendicular planes, with 64 vertical and 64 horizontal scintillators. Each channel is ended by PMTs, which accept signal via plexiglas light guide [3]. The planes are divided into four quadrants with 16 scintillators each, as we can see in Figure 10.1.

10.2 CHOD and L0 trigger level

Some photons from the π^0 decays can convert or undergo photonuclear interactions and create low energy hadrons in RICH mirror plane, which amounts radiation lenght about 20%. The simulations have shown that these photons can increase the inefficiency of the LKR, which must not be worse than 10^{-5}. To avoid this increase, some detector between RICH and LKR is needed. This satisfy the CHOD, which detects the low momentum charged tracks. The CHOD is a great complementary detector at L0 trigger level to the RICH, because it has a time resolution about 200 ps. The particle flux rate in the CHOD is estimated to be around 11 MHz [3].

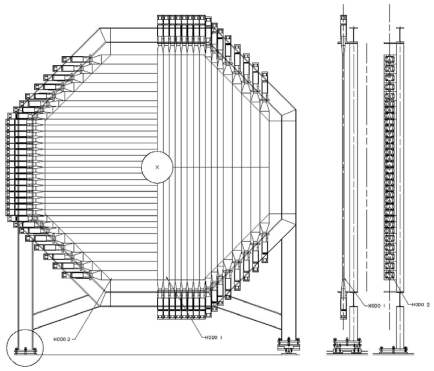

Figure 10.1: Schematic view of the CHOD.[3]

11. Liquid Krypton calorimeter (LKR)

11.1 Introduction

The Liquid Krypton calorimeter used in this experiment is an electromagnetic calorimeter. The electromagnetic calorimeters are designed to measure an energy deposition of electrons and positrons in the volume of the calorimeter. When some particle hits the active volume of the calorimeter and have an appropriate energy, it creates an electromagnetic shower via multiple electromagnetic interactions in active volume. Only the electromagnetic calorimeters can be homogenous, what means we have same material in the whole calorimeter volume. The LKR is homogenous and this property is very usefull, because the whole volume is active and we are not losing an undetectable energy in passive absorbers. In our case the tank is of course filled with liquid krypton, so the krypton is both the active material and the absorber.

11.2 Data from 2006 run

In 2006 some efficiency measurements were made, which used NA48 apparatur. These measurements used 25GeV electrons, that can interact with the upstream apparatus and create bremsstrahlung photons. The electrons are deflected due to spectrometer magnets, so they hit different cells than photons. Typically there is no difference in y direction and about 12 cm in x direction [31]. Figure 11.1 shows the positions of the clusters in a typical event.

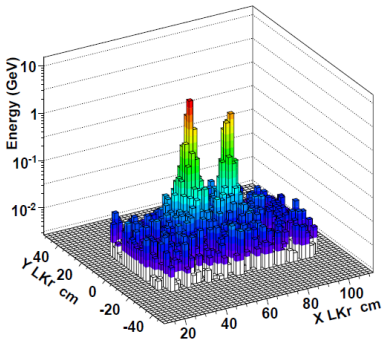

Figure 11.1: Typical positions of the clusters.[31]

12. The Muon Veto Detector (MUV)

12.1 Introduction

The MUV has to suppress the muon events at the first trigger level already by factor of about 20 and reject the charged particles traversing through the iron plate. It also has to suppress the electromagnetic showers, which are born by bremsstrahlung in iron plate and distinguish them from the hadronic pion showers by masurements of shower shape. Because of that we need a sufficient segmentation of the calorimetric system. So we need a fast veto detector with a time resolution better than 1 ns to reject the events with coincidence signals in the Gigatracker and the CEDAR.

12.2 Components of the MUV

The muon veto system consists of three distinct detectors MUV1, MUV2 and MUV3. The MUV1 follows directly the LKR calorimeter and together with the MUV2 are hadron calorimeters. While the MUV1 module is new, the MUV2 is reused from the NA48 experiment and is only rotated by 180°, because of alignment. After these two modules follows the 80cm thick iron layer and after that is the last detector in the experiment, the MUV3 or the fast muon veto. The MUV1 and the MUV2 are classic iron sandwich hadrons calorimeters with 24 and 22 layers of scintillator strips. The first module allows a better distinction between the hadronic pion and the electromagnetic muon showers.

The last module MUV3 is new, only the photomultipliers (PMT), which have been tested in Mainz [32], are from previous experiments. It consists of 148 separated chambers, each eqiupped with two PMTs. The chambers are deployed homogenous, only just near the beam are concentrated. When the particle activates the scintillator it takes a little time to emit photons, so when the particle is passing through the window of PMT there are some emitted photons due to photo effect which hit the dynode of the PMT and we detect the signal earlier than from the scintillator. Because we need a very accurate time resolution, we need to have two PMT in each chamber. Through the modules passing the central beam hole with a diameter of about 212 mm.

The scintillators used in the MUV1 are made of polystyrene (Styron 143E) as

carrier substrate with 2% scintillating fluors (p-terphenyl) and 0.05% POPOP. While the p-terphenyl emits scintillation light at about 300 – 400 nm in the ultra-violet, POPOP shifts the wavelength to 380 – 500 nm. The procedure used to fabricate the scintillators is as follows: the mixture of polystyrene pellets, p-terphenyl, and POPOP is melted under a 10-4 bar vacuum at about 250 °C. This procedure allows the fabrication of large numbers of long scintillator strips in a relatively short time. One production cycle of heating, melting and cooling needs about 14 hours. In the MUV2 are scintillators from original NA48 experiment. The MUV3 contains scintillators made of the same mixture as the MUV1, only as the production technique is used polymerisation [3]. Scintillators are produced at IHEP in Protvino.

13. Conclusion

In this thesis I tried to describe the NA62 experiment in CERN and its importance in modern physics. Both, the physical motivation and description of detectors have place in this thesis. This experiment has great potential to verify the Standard Model or to point out some theory beyond the SM, for example natural SUSY. But there are more interesting theories, that could be explored with the NA62 equipment.

To better understand the experiment theory, used detectors and their cooperations, I have joined the NA62 experiment group for one month. I am assigned to the Straw Tracker Working Group. Partially I have helped with processing data from aging tests. Then I also joined a MUV Working Group, where I helped with assembling the MUV3 module. In the future I am going to continue working on this experiment.

Bibliography

[1] http://na48.web.cern.ch/NA48/Welcome/papers/Overview.html#04

[2] Test of Lepton Flavour Universality in $K^+ \to l^+\nu$ Decays :
Phys. Lett. B698

[3] NA62 Collaboration **Technical Design Document** NA62-10-07,
December 2010

[4] 2011 Review of Particle Physics. K. Nakamura et al. (Particle Data Group),
Journal of Physics G37,
075021 (2010) and 2011 partial update for the 2012 edition.

[5] N. Craig, M. McCullough and J. Thaler,
"Flavor Mediation Delivers Natural SUSY", arXiv:1203.1622 ,[hep − ph].

[6] Report from the Physics WG,
Presentation by Giuseppe Ruggiero - NA62 Analysis meeting, 29.3.2012

[7] Rare decays and MSSM phenomenology, Presentation by Andreas Crivellin,
ITP Bern, 07.03.2012

[8] Yukawa coupling and the CKM-Matrix, Presentation by Nicolas Kaiser,
23.11.2010

[9] Jiří Hořejší - Fundamentals of Elektoweak Theory, The Karolinum Press,
Prague 2002

[10] Michael E. Peskin Daniel V. Schroeder - An Introduction to Quantum Field
Theory, Perseus Books Publishing, Massachusetts US 1995

[11] A. Ceccucci, Z. Ligeti and Y. Sakai,"The CKM quark-mixing matrix",
CITATION = INSPIRE-806139

[12] Heavy Flavor Averaging Group, E. Barberio *et al.*, arXiv:0808. 1297,
and Summer 2009 updates at http://www.slac.stanford.edu/xorg/hfag/.

[13] A. V. Artamonov et al. [E949Collab.], Phys. Rev. Lett. 101, 191802 (2008)

[14] G. Anelli et al., "Proposal to Measure the Rare Decay $K^+ \to \pi\nu\bar{\nu}$",
CERN-SPSC-2005-013, SPSC-P-326, 11/06/2005.

[15] Some experimental remarks on K_L, K^+ rare decays, Presentation by C.Lazzeroni, University of Birmingham and G.Ruggiero, Scuola Normale Pisa, NA62 Physics Handbook meeting at CERN - 10.-12. Dec. 2009

[16] Overwiev about hyperons, Presentation by Lisheng Geng, IFIC, Valencia University, Spain,
NA62 Physics Handbook meeting at CERN - 10.-12. Dec. 2009

[17] Rare Kaon Decays: Standard Model Predictions, Joachim Brod, Presentation by TU München, TUM-IAS,
NA62 Physics Handbook meeting at CERN – 10.-12. Dec. 2009

[18] From radiative to rare decays, Presentation by Christopher Smith,
NA62 Physics Handbook meeting at CERN – 10.-12. Dec. 2009

[19] Hadronic physics "experimental" issues, Presentation by M. Sozzi,
NA62 Physics Handbook meeting at CERN – 10.-12. Dec. 2009

[20] Non-Leptonic Kaon Decays: Direct CP Violation, Presentation by Joaquim Prades, CAFPE and Universidad de Granada, NA62 Physics Handbook meeting at CERN – 10.-12. Dec. 2009

[21] Radiative decays - Theory I, Presentation by Giancarlo D'Ambrosio, INFN-Sezione di Napoli,
NA62 Physics Handbook meeting at CERN – 10.-12. Dec. 2009

[22] E. Abouzaid *et al.* [KTeVCollaboration], "Measurement of the rare decay $\pi^0 \to e^+e^-$",
Phys. Rev. D **75** (2007) 012004
[hep − ex/0610072]. CITATION = HEP-EX/0610072

[23] The NA62 Detector, Presentation by Ferdinand Hahn,
NA62 Physics Handbook meeting at CERN – 10.-12. Dec. 2009

[24] C. Bovet, et al.: The CEDAR Counters for Particle Identification in the SPS Secondary

[25] NA62 Collaboration, 2012 NA62 Status Report to the CERN SPSC

[26] NA62 Collaboration, 2011 NA62 Status Report to the CERN SPSC

[27] **OPAL Collaboration, K. Ahmet et al.**
Nucl. Instrum. Methods A, 305 (1991) 275. 1991, Vol. 305, p. 275.

[28] Straw Tracker, Presentation by Hans Danielsson,
WG meeting at CERN - 26.3.2012

[29] T. AKESSON ET AL. Aging studies for the ATLAS Transition Radiation Tracker (TRT).
Nuclear Instruments and Methods in Physics Research Section A: Accelerators, Spectrometers, Detectors and Associated Equipment,
v. 515, n.1-2, p. 166-179, December 2003

[30] Anzivino, G. et al., Construction and test of a RICH prototype. Nucl. Instrum. Methods A593. 2008, pp. 314-318.

[31] Na62 Collaboration, 2007 NA62 Status Report to the CERN SPSC

[32] http://na62-muv1.physik.uni-mainz.de/muv3/muv3_pms.html